Robotica (2010) volume 28, pp. 369–379. © Cambridge University Press 2009
doi:10.1017/S0263574709005694

# Experimental evaluation of open-loop swimming control for a robotic fish using electrostatic film motors

Norio Yamashita†, Zu Guang Zhang‡*, Akio Yamamoto†, Masahiko Gondo§ and Toshiro Higuchi†

†*Department of Pricision Engineering, Graduate School of Engineering, The University of Tokyo, Tokyo, Japan*
‡*Department of Mechanical Engineering, Faculty of Science and Technology, Tokyo University of Science, 2641 Yamazaki, Noda, Chiba 278-8510, Japan*
§ *SEIDENSHA Corporation, SIC-2-404, 5-4-21 Nishi-Hashimoto, Sagamihara, Kanagawa, Japan*

(Received in Final Form: April 14, 2009. First published online: June 3, 2009)

**SUMMARY**

We have developed an underwater robotic fish using a unique three-layer electrostatic film motor. In the robotic fish, the unique motor actuates a flexible caudal fin to propel the robot via an elaborate power transmission system. In the present study, we describe the major disadvantages of the previous prototype of the robotic fish and improvements of the prototype. In addition, we present experimental evaluations related to the control parameters and locomotion performance of the robotic fish. These control parameters include the frequency and initial phase of AC voltage, and the amplitude and period of frequency sweeping. A simple theoretical model concerning the power transmission system of the robotic fish is also analyzed to provide a possible explanation for the unique swimming control. By appropriately adjusting these control parameters, we achieve cruising, emerging, submerging, and turning of the robotic fish even though only the caudal fin is active. Finally, we show smooth human-operated turn-around motion similar to that seen in real fish. Based on these experimental results, we further clarify the relationships between the open-loop motor pattern and motion parameters.

KEYWORDS: robotic fish; 3-lyaer electrostatic film motor; power transmission model; open-loop swimming control; experimental evaluation.

## 1. Introduction

Fish are highly maneuverable and power-efficient endurance swimmers. A traditional classification scheme[1] of fish locomotion broadly identifies two swimming styles: (1) body and/or caudal fin (BCF) locomotion and (2) median and/or paired fin (MPF) locomotion. Fast-swimming fish (e.g., tuna and sharks) that have very low-drag body shapes, narrow peduncles, and tall lunate caudal fins, propel themselves only through oscillations of caudal fins.[2] Thus, the BCF swimming is considered to be the most efficient at cruising speeds.[3]

Such astonishing swimming ability of fish have inspired researchers to improve the performance of autonomous underwater vehicles in terms of efficiency and maneuverability. Perhaps the most notable early example of an underwater vehicle capable of fish-like swimming was developed by MIT in the early 1990s.[4] Other robotic fish have been developed, including the famous Mitsubishi robotic fish[5] and Hirata's prototypes.[6] Hu *et al*. developed two series of robotic fish: the G series and the MT series.[7,8] In particular, their MT series robotic fish with a "single-motor-multi-joint" tail structure realized many fish-like motion, such as C-shape sharp turning and S-shape fast starting. Based of a biological concept, the Biological Inspired Robotic Group (BIRG) at Ecole Polytechnique Fédérale de Lausanne (EPFL) implemented swimming and crawling in a robotic fish.[9] They designed a control architecture based on a central pattern generator (CPG) to produce coordinated patterns of rhythmic activity. One recent design is the micro autonomous robotic ostraciiform (MARCO), the design of which is inspired by highly stable and fairly maneuverable boxfish.[10] A number of robotic fish use electromagnetic motors for propulsion, including the above-mentioned prototypes. However, Barrett *et al*.[11] reported that the actuation of electromagnetic motors is noisy and requires a fairly elaborate transmission system to amplify torque. As a result, several researchers have recently published research applying unique actuators (e.g., shape memory alloy actuator, piezoelectric actuator, and conducting polymer actuator) to robotic fish as artificial muscles.[12–16]

The present study focuses on the realization of fish-like mobility using the oscillation of a flexible caudal fin and making our robotic fish more like a natural fish. Our work started with some researches on a light, thin, and flexible actuator called an electrostatic film motor.[17–19] Since the electrostatic film motor can normally operate even though being bent into a horseshoe shape, it is adequate for light and flexible mechanisms, such as artificial muscles. Inspired by this idea, we fabricated a robotic fish using this unique actuator. The body of the first-generation prototype[20] consists of two flexible printed circuit (FPC) films (i.e., a stator and a slider of the electrostatic film motor). Namely, the actuator is used directly to construct the fish body and exposed to outside. Since the electrostatic film motor requires a dielectric liquid, such as silicon oil or Fluorinert, as a

* Corresponding author. E-mail: hero@rs.noda.tus.ac.jp

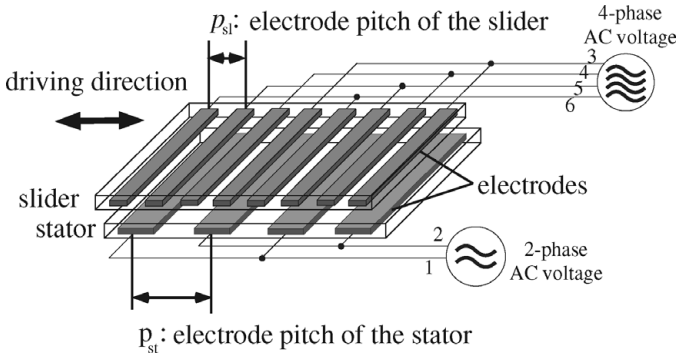


Fig. 1 Schematic diagram of the two-four-phase electrostatic film motor. The motor is a synchronous motor having two-phase and four-phase electrodes configured within two flexible printed circuit films called a "stator" and a "slider," respectively.

surrounding medium due to an electric discharge problem, the first robotic fish cannot work in water, necessitating the use of a dielectric fluid as a swimming medium. Another limiting factor in the design of the first prototype has been its use of the large-sized controller scheme. Therefore, we designed an improved prototype[21] in which a fish-like waterproof coat was fashioned of silicon rubber and a compact control system was constructed. To avoid a resultant discharge in the air gap between the stator and slider films of the electrostatic motor, we injected silicon oil into the waterproof coat so that the gap is filled with the oil. The main disadvantage of the second-generation prototype is that the silicon oil gradually permeates the waterproof coat made of silicon rubber due to their affinity.

To this end, we have centered our attention on the design features and system configuration of the robotic fish proposed in our previous studies. However, we have not yet evaluated the swimming capability of the newly designed robotic fish in detail. In the present paper, we introduce an improved prototype robotic fish, which can be stably employed in a long-term experiment. Furthermore, we use a motion-capture system to evaluate the operation properties of the redesigned robotic fish for the first time. In the following section, we review the operation principle of the electrostatic film motor and describe the three-layer structure that is employed in the robotic fish. Then, Section 3 describes the improved design of the robotic fish. The motion of the newly developed fish in an aquarium is examined in Section 4, which shows the relationships between the open-loop motor pattern and the fish locomotion parameters.

## 2. Electrostatic Film Motor

### *2.1. Essential structure*

In order to expressly understand the operation principle of the unique actuator, we first explain its properties using an essential structure. Figure 1 shows a schematic diagram of the essential structure, which can be regarded as a synchronous motor having two-phase electrodes for a stator and four-phase electrodes for a slider, both configured within flexible printed circuit films. The electrode pitch for the stator $p_{st}$ is designed to be twice as large as that for the slider $p_{sl}$, so that the resultant cycle lengths of the voltage signals become the same. In order to decrease the influence of friction between the slider and the stator, glass beads of 7 μm in diameter are scattered between the two films. While the slider film is placed directly on the stator film, it is driven by the electrostatic force to accomplish the linear motion. The slider and stator are excited by four-phase and two-phase AC high voltages, respectively. Note that the electrostatic film motor usually operates by high voltages of over 1 $kV_{0-p}$ so as to obtain a practical electrostatic force. In general, the electrostatic field between the films will exceed the maximum field strength of air under such high voltages so that a resultant discharge can occur in the air gap, which is not desirable. Thus, a dielectric liquid (e.g., silicon oil) should be injected into the gap between the stator and slider films in order to avoid the undesirable discharge.

The motor is excited by a set of two-phase and four-phase AC voltages. The voltages of the six phases can be expressed in vector form as follows:

$$\begin{aligned}\mathbf{v} &= [v_1, v_2, v_3, v_4, v_5, v_6]^T \\ &= \Big[\, v_{st}\sin(2\pi f_{st}t), -v_{st}\sin(2\pi f_{st}t), \\ &\quad v_{sl}\sin(2\pi f_{sl}t), v_{sl}\cos(2\pi f_{sl}t), \\ &\quad -v_{sl}\sin(2\pi f_{sl}t), -v_{sl}\cos(2\pi f_{sl}t)\,\Big]^T, \end{aligned} \tag{1}$$

where $v_1 \sim v_6$ represent the voltages applied to the corresponding electrodes, $v_{st}$ and $v_{sl}$ represent the voltage amplitudes, and $f_{st}$ and $f_{sl}$ represent the frequencies of the AC voltages on the stator and the slider. As reported in our previous papers,[19,21] the slider can be synchronously driven by the two reverse frequency components (e.g., $f_{st} + f_{sl}$ and $f_{st} - f_{sl}$). In addition, we can virtually eliminate the component of the sum when we use high-frequency AC signals. In our experiments, the slider running speed $u$ is governed only by the component of the difference of the frequencies because the relatively high frequency are applied, and can be written as

$$u = 2p_{st}f_{st} - 4p_{sl}f_{sl}. \tag{2}$$

Under the synchronous driving, the maximum thrust force is approximately proportional to the product of amplitudes, $v_{st}$ and $v_{sl}$.[19] In addition, in the previous study, we reported that the maximum thrust force of approximately 0.3 N can be obtained while the voltage amplitudes $v_{st}$ and $v_{sl}$ are 1 kV.

### *2.2. Three-layer structure*

We have proposed an elaborate three-layer motor structure for our robotic fish to enhance the thrust of the motor.[21] Figure 2 shows the structure of the three-layer motor in which a dual-side two-phase electrode film is defined as a stator film and clamped by two pieces of single-side four-phase electrode film, which are referred to as slider films. It is important to note that only one set of four-phase AC voltages is applied to the sliders, even though there are two pieces of slider film. As shown in Fig. 2, we can apply AC voltages to one slider film only by reversing the connection of a set of four-phase AC voltages applied to each other. Thus, the slider running speed on one side is always opposite to that

https://doi.org/10.1017/S0263574709005694 Published online by Cambridge University Press

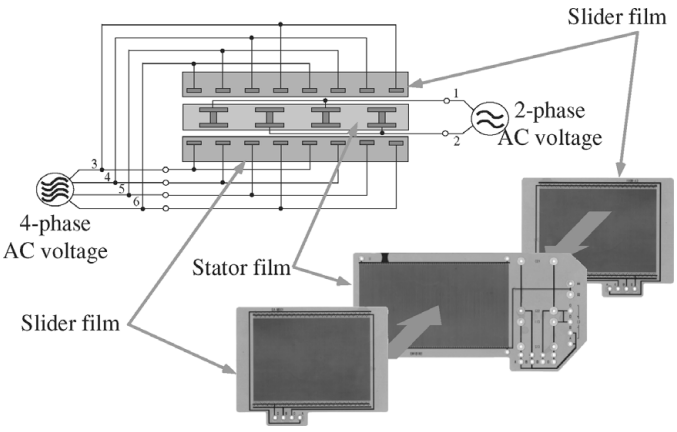


Fig. 2 Schematic diagram of the three-layer motor. A dual-side two-phase electrode film is clamped between two single-side four-phase electrode films. The stator and sliders are excited by a set of two-phase and four-phase high AC voltages, respectively.

on the other side. As a result, when one slider moves forward at a certain speed, the other will move backward at the same speed. The approach simplifies the supply of the control signals and facilitates the fabrication of the control system. Such a reciprocating motion of the sliders will be converted into the swing of the caudal fin of the robotic fish, which will be described in the next section.

## 3. Robotic Prototype

### *3.1. Mechanical redesign*

In our previous research on the second-generation robotic fish,[21] we shaped a waterproof coat out of silicon rubber so that the robotic fish could swim in water. Since the motor requires dielectric liquid as its surrounding medium in order to avoid the undesirable discharge, we injected silicon oil into the waterproof coat. However, the robotic fish worked well only during a short period of approximately four weeks under this approach. In a long-duration experiment, silicon oil permeates the waterproof coat made of the silicon rubber by degrees due to their chemical affinity. The waterproof coat then cracked after gradually soaking up the silicon oil, as shown in Fig. 3(a). Another shortcoming in the previous design of the second-generation robotic fish was the alignment of films in the three-layer electrostatic film motor.

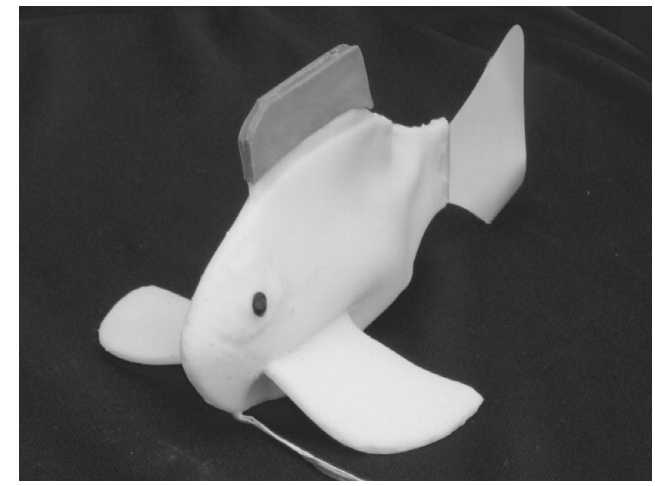

Fig. 4 Improved robotic fish with a waterproof coat made of polyurethane rubber.

Figure 3(b) shows the previous mechanical configuration of the power transmission system employed in our robotic fish. An undesirable pitch angular deflection was sometimes observed between the stator film and slider films, probably due to disturbance of the mechanisms. Once such a deflection occurs, the motor cannot operate normally, resulting in paralysis of the caudal fin.

In the present paper, we focus on solutions of the above-mentioned problems and present an improved version of our robotic fish. The use of silicon oil is preferred based on its insulation performance and relative density with respect to water. Therefore, the waterproofing material was changed to polyurethane rubber based on its oil resistance properties. According to the results of an oil resistance test, we verified that the silicon oil barely permeates the polyurethane gum. Figure 4 shows the new robotic fish prototype with a waterproof coat of polyurethane gum. The size of the robotic fish is identical to that of the previous prototype (i.e., 175 mm × 95 mm × 100 mm) and its total weight is approximately 82 gm. The new robot is lighter than the previous robot. The lighter body facilitates the improvement of the locomotion performance of the robotic fish, especially the performance of turning in water.

Figure 5 shows the internal mechanism of the prototype robot. In this prototype, we elaborated linear guides to avoid

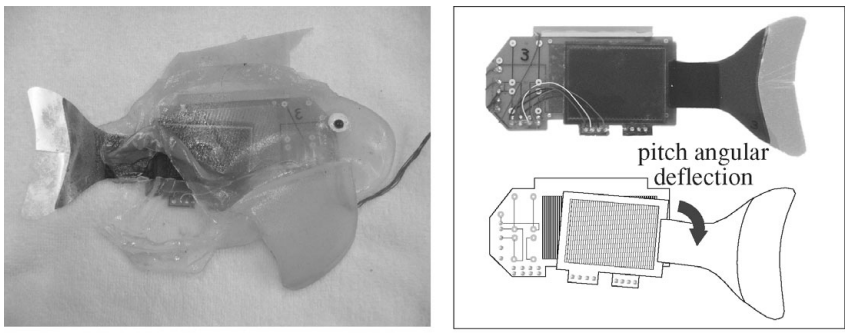


(a) (b)

Fig. 3 Limitations of the second-generation robotic fish: (a) the waterproof coat cracks easily after gradually soaking up silicon oil; (b) the motor cannot propel the caudal fin due to the undesirable pitch angular deflection between the stator and slider films.

https://doi.org/10.1017/S0263574709005694 Published online by Cambridge University Press

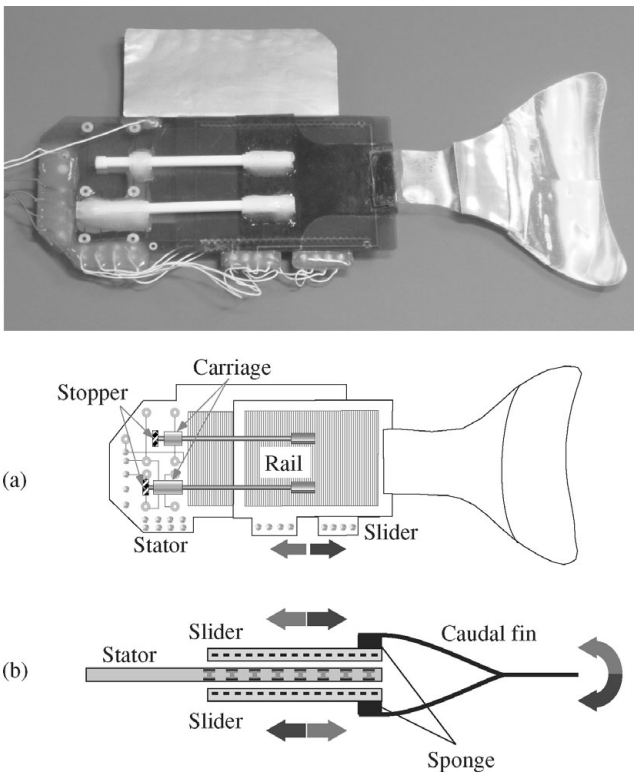


Fig. 5 Linear guide for the three-layer electrostatic film motor. This prevents the pitch angular deflection of the slider films and limits their reciprocating motion to a route parallel to the rails.

the pitch angular deflection between the stator and slider films that was observed in the previous robot. As shown in Fig. 5(a), two rails are fixed to the slider film, and carriages are fixed to the stator film. A stopper is attached to the end of a rail to preclude disengagement. As a result, the alternating push–pull motion of the slider films is limited to a route parallel to the rails. This effectively prevents the pitch deflection of slider films and ensures smooth operation of the motor. Thus, the push–pull motion of the two slider films is converted into the swing motion of the caudal fin in the same manner as same as the previous prototype. As shown in Fig. 5(b), the caudal fin made of plastic film was glued to the ends of the two slider films so that the push–pull motion is transformed into lateral swinging motion of the fin.

### *3.2. Swimming control method*

The muscle functions of living fish include both extensor and flexor functions.[22] To imitate muscle-like activation patterns, we should accomplish the reciprocating motion on the three-layer electrostatic film motor. Furthermore, a smooth speed modulation is required because the unique motor will step out if the slider running speed is changed excessively. Therefore, we engaged the following frequency modulation to realize smooth reciprocating motion:

$$f_{\mathrm{st}}(t) = A \sin\left(\frac{2\pi}{T_{sw}} t\right) + f_{\mathrm{const}},$$
$$f_{\mathrm{sl}}(t) = f_{\mathrm{const}}, \qquad (3)$$

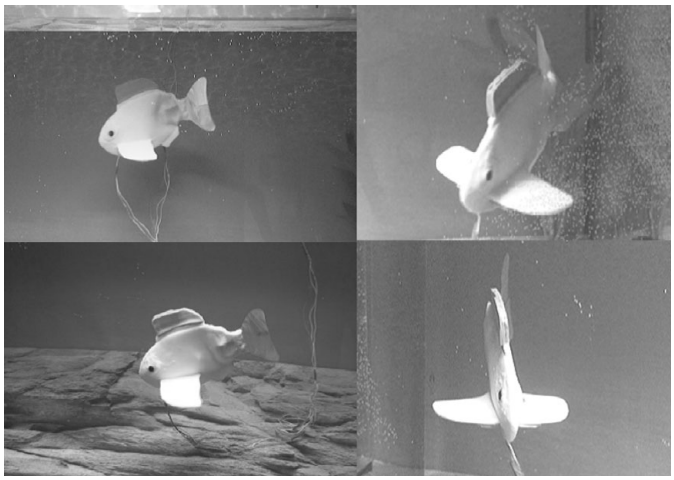

Fig. 6 Swimming motions of the robotic fish. These pictures show right turning (upper right), left turning (lower right), swimming near the surface (upper left), and swimming near the bottom (lower left).

where $f_{\mathrm{const}}$ is a constant frequency, $A$ is the amplitude of frequency sweeping, and $T_{\mathrm{sw}}$ represents the sweeping cycle period.

## 4. Experimental Results and Analyses

In this section, we describe relations between motor control parameters and locomotion of the fish robot. The swimming speed, turning performance, and submerging performance of the fish robot have been investigated. Figure 6 shows snapshots of some of the basic motions of the new prototype robot. The robotic fish is capable of cruising in an aquarium with turning, emerging, and submerging motions.

### *4.1. Experimental setup*

The experimental setup for driving the fish robot is shown in Fig. 7. To generate high-frequency high voltages, a combination of high-speed amplifiers (HSA4012, NF circuit block, voltage gain: 10) and transformers that have 1:33 turns ratio are utilized. One amplifier, which is connected to two transformers, supplies two outputs with reversed phases. The amplitude of the voltages was fixed at 1 $kV_{0-\mathrm{p}}$ in all the experiments. The fish robot was placed in an aquarium having a size of 0.45 m × 0.90 m × 0.45 m. The three-dimensional motion of the fish robot was measured by a motion capture system (LIBRARY Co.). The position data of the robotic fish were calculated by tracking black markers attached to the body with two video cameras. Velocity was calculated by taking the derivative of the position data.

### *4.2. Swimming mode*

Since only the caudal fin can be actively actuated in the robotic fish, all of the motions are generated by adjusting various patterns of the caudal fin motion. In order to investigate the swimming mode, we observed the motions of passive parts of the body. A photograph showing the trajectories of the head, dorsal fin, and body is shown in Fig. 8. Although slight oscillations of the head and dorsal fin were observed, almost no oscillations appeared at the center

https://doi.org/10.1017/S0263574709005694 Published online by Cambridge University Press

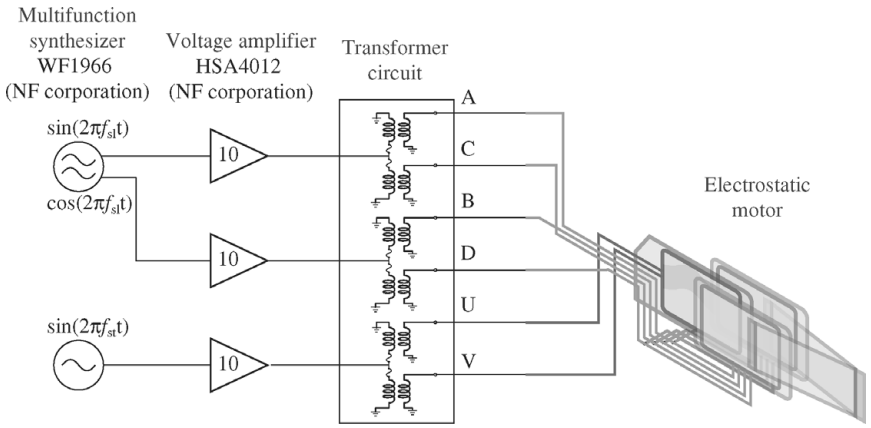


Fig. 7 Schematic diagram of the driving system. Sinusoidal signals generated by the function generator are amplified by 330 times as a whole.

of the body. Such a swimming mode is defined as carangiform swimming, which is adopted by some faster swimming fish, as indicated in the literature.[3]

### *4.3. Cruising speed*

For a straight cruise, the caudal fin equably swings to the right and left sides. The cruising speed of the robotic fish depends on the swing period and the swing speed of the caudal fin, which are controlled through the motion of the electrostatic film motors (see Appendix A for details). The cruising speed was measured at various amplitudes of frequency sweeping (i.e., $A$ in Eq. (3)) and sweeping cycle period (i.e., $T_{sw}$ in Eq. (3)). In these experiments, the frequency on the slider (i.e., $f_{const}$ in Eq. (3)) was fixed at 2000 Hz. As shown in Fig. 9, the maximum cruising speed was observed to be approximately 70 mm/s. In simplified terms, it may be seen that the robotic fish will accelerate as the amplitude of frequency sweeping increases until a certain point, at which its velocity causes the drag force to equal the propulsion force. After this point, the robotic fish will no longer accelerate, but will cruise at a constant velocity or slightly decelerate. Note that the wider swing

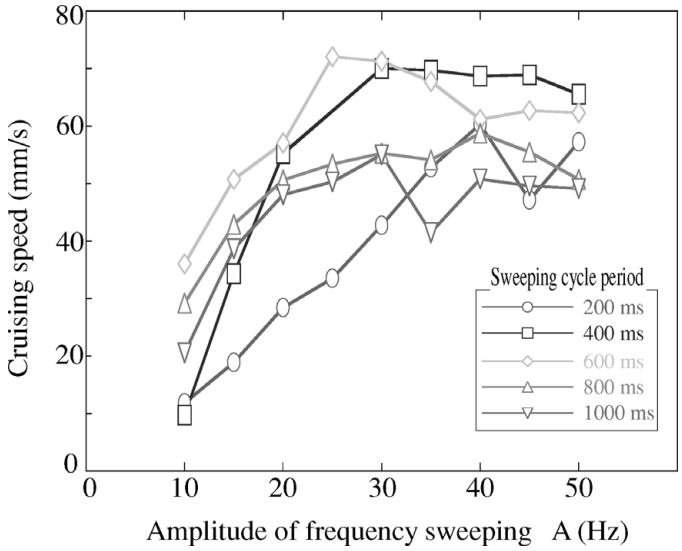


Fig. 9 Swimming speed of the fish robot in open-loop control.

motion of the caudal fin generated by the larger amplitude of frequency sweeping causes the obvious swaying motion

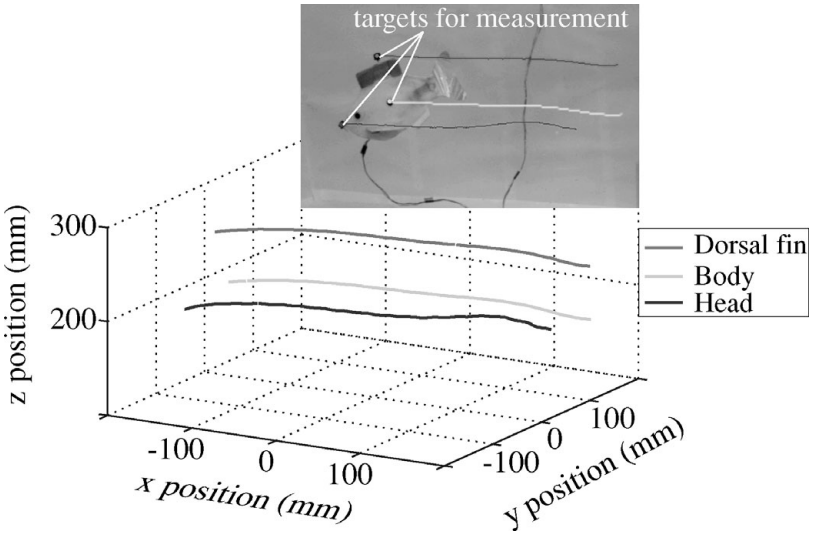


Fig. 8 Captured motion and the trajectories of targets.

https://doi.org/10.1017/S0263574709005694 Published online by Cambridge University Press

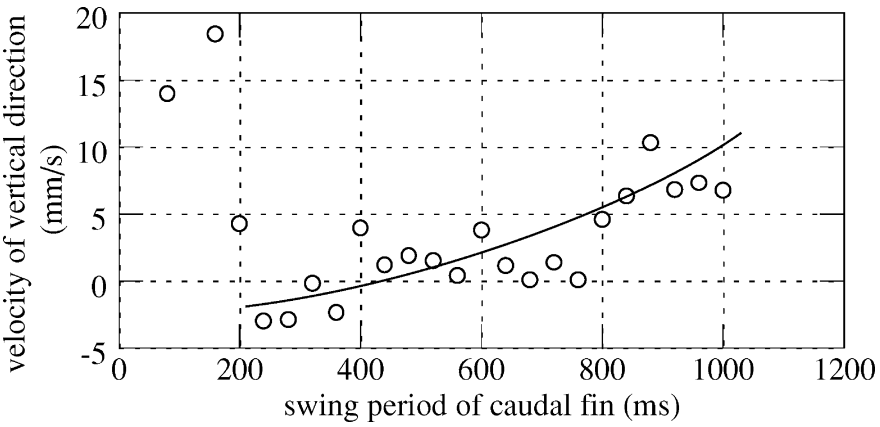


Fig. 10 Vertical speed.

of the head. Thus, the effective surface area exposed to the liquid in the direction of motion is increased so as to cause the larger drag force. In addition, the excessively wide and fast movement of the slider of the electrostatic film motor results in the large displacement and large reactive force from the waterproof coat, which might cause the step-out of the motor. As discussed in Appendix B, the thrust force of the electrostatic film motor sufficient to the workload of the caudal fin is theoretically analyzed.

### *4.4. Emerging and submerging motion*

Since its buoyancy is adjusted to be larger than gravity, the robotic fish will emerges toward the water surface if it does not or less propel. In contrast, the robotic fish can gradually submerge when the downward propulsion is sufficient because its head is inclined down. The relationship between the motor operation parameters and the emerging motion of the robotic fish has been examined, as shown in Fig. 10. In these experiments, the frequency $f_{sl}$ applied to the slider was fixed at 2000 Hz and the amplitude of frequency sweeping $A$ was set as 25 Hz. When the swing period of the caudal fin was less than 200 ms, the swing amplitude of the caudal fin was very small and the propulsion force was small. As a result, the robotic fish emerged almost vertically and did not swim forward. Between 200 ms and 400 ms, the robotic fish submerged by degrees because propulsion sufficient to counteract the effect of buoyancy was provided. Although the locomotion of the robotic fish trended upward under a swing period greater than 400 ms, it still moved forward.

Figure 11 shows three trajectories tracked by the marker attached to the dorsal fin under three swing periods of the caudal fin (i.e., 280 ms, 560 ms, and 800 ms). At 280 ms, the robotic fish submerged since the propulsion could counteract the effect of buoyancy. At 560 ms, it almost maintained horizontal swimming. At 800 ms, the robotic fish gradually emerged. Note that the cruising speed at 560 ms was the fastest of the three cases. It means that propulsion provided by oscillating of the caudal fin is mostly consumed to drive the robotic fish forward. In the case of swing period 800 ms, an obvious swaying motion of the head was observed due to the larger swing period. Such swaying motion caused the larger drag force so that the cruising speed of the robotic fish decreased because propulsion had to counteract the increasing drag force. Even though all of the fins of the robotic fish except the caudal fin were inactive, the robotic fish could realize cruising motion in a horizontal plane, as well as emerging and submerging motions, by adjusting the swing patterns of the caudal fin.

### *4.5. Turning motion*

Although the first-generation prototype achieved turning motion by oscillating the caudal fin while shifting the neutral point,[20] it is unnecessary to use such method in the present robot because of large moment of inertia caused by the

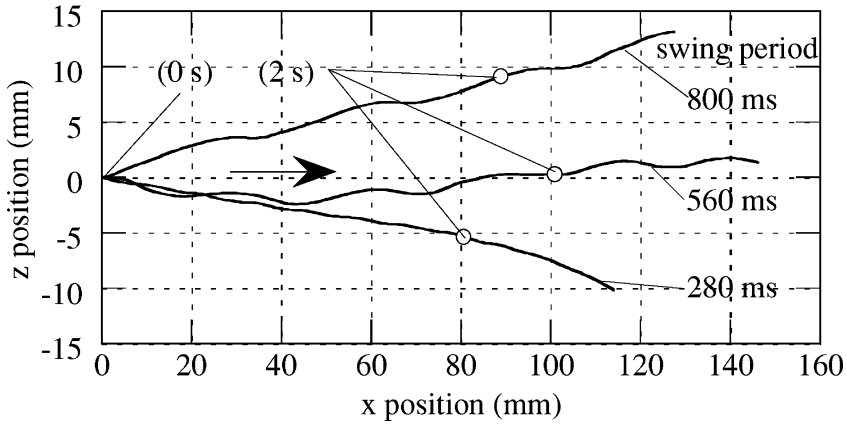


Fig. 11 Trajectories of cruising, emerging, and submerging.

https://doi.org/10.1017/S0263574709005694 Published online by Cambridge University Press

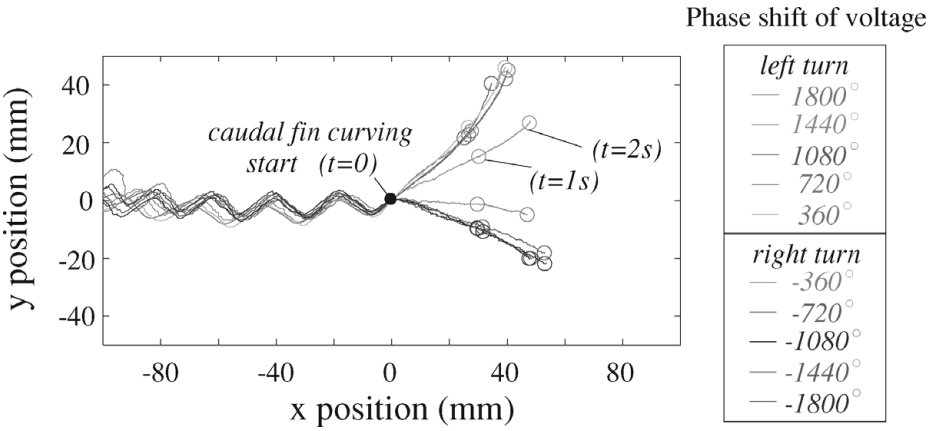


Fig. 12 Relationships between phase deviation and turning trajectories. Angles are the phase shift of the stator voltage.

relatively large mass of the robot. It is suitable for the new robotic fish to use another turning method in which the caudal fin is kept at a constant angle to form a curved fish shape. Under the influence of the inertia and interaction between the compliant body and surrounding water, the robotic fish can accomplish a C-shape turning. But, such turning motion is comparatively slow. In the practical operates, we can accelerate turning motion by repeating curve motion of the caudal fin.

In order to evaluate the turning properties of the robotic fish, we have studied the relationship between the deformation of the caudal fin and turning motion. In the control of the turning motion, the frequencies of AC voltages applied to the stator and slider films (i.e., $f_{\mathrm{st}}$ and $f_{\mathrm{sl}}$) are first fixed at 2000 Hz. Namely, the slider of the electrostatic motor remains static and the caudal fin does not swing. The slider then starts to move by varying the initial phase $\phi$ of AC voltages on the stator, as formulated in Eq. (4). In our experiments, five different target phases were selected with a $2\pi$ step for the left- and right-turning directions:

$$
\begin{aligned}
v_1 &= v_{\mathrm{st}} \sin(2\pi f_{\mathrm{const}} t + \phi),\\
v_2 &= -v_{\mathrm{st}} \sin(2\pi f_{\mathrm{const}} t + \phi).\\
\phi &= \begin{cases} 20\pi t \ \ (\text{until } \phi \text{ reaches the target value, } \phi_{\mathrm{ref}}) \\ \phi_{ref} \ \ (\text{after } \phi \text{ reaches } \phi_{\mathrm{ref}}) \end{cases}. \qquad (4)
\end{aligned}
$$

As mentioned above, turning motion generated by a single curving of the caudal fin is too inappreciable to observe the curvature of turning trajectory. Therefore, we make the robotic fish swim straightly before turning in order to obtain sufficient inertia. As a result, the curvature of turning trajectory sufficient for experimental observation occurs. The trajectories tracked by the marker attached to the head of the robotic fish for the duration of turning motion are plotted in Fig. 12. The left parts of the plot represent the trajectories of straight swimming. At the origin, the robotic fish started to bend the body into a curved shape based on the above-mentioned turning method. Approximately one second later, the robotic fish began to turn under the influence of inertia and interaction between the compliant body and surrounding water. Moreover, the curvature of the turning trajectories has already been calculated, as shown in Fig. 13. There is no large difference in the curvature among the various phase shifts. This suggests that controlling the turning curvature with accuracy is impossible in the proposed turning method. Based on our experimental observation, the robotic fish frequently became stationary before finishing a whole turning motion. The reason for this is that the implemented turning method relies on inertia alone and does not generate any propulsion force for the duration of turning. In addition, the physical property of the waterproof coat material has possibly a negative effect on the turning motion.

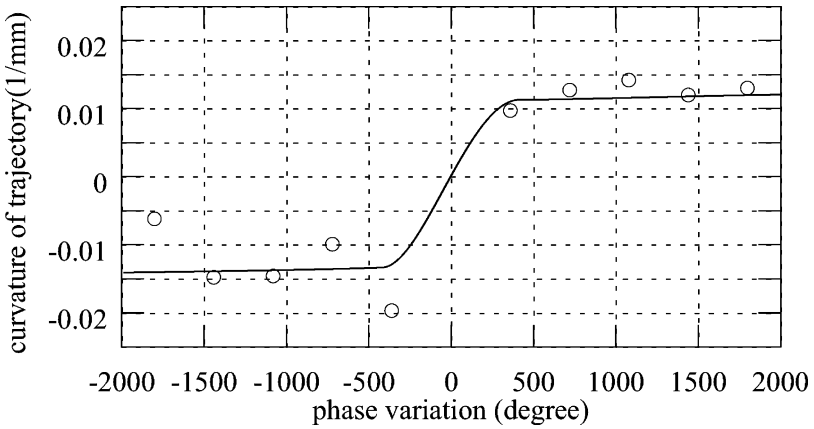


Fig. 13 Curvature of turning trajectory.

https://doi.org/10.1017/S0263574709005694 Published online by Cambridge University Press

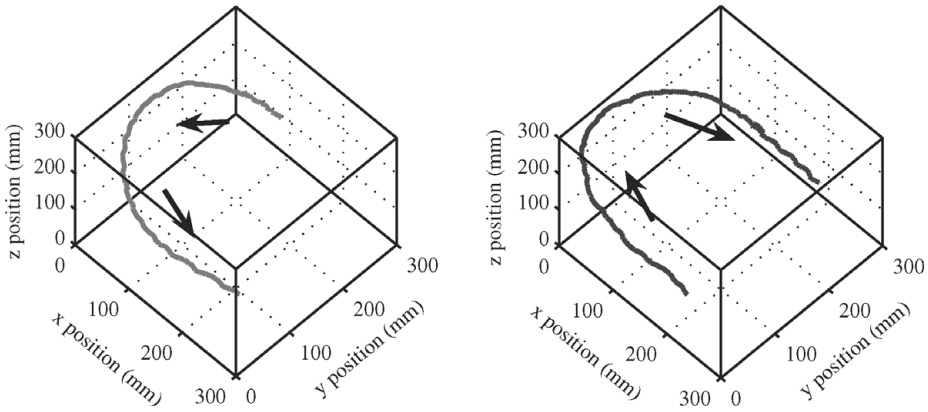


Fig. 14 C-shape turning of fish robot by human operation. The trajectories with smooth C-shape turning showed high maneuverability of the fish robot.

In general, practical turning, such as a turnaround, can be achieved by a few repetitive cycles of intermittent swinging and bending the caudal fin, which will be described in detail in the next section.

### *4.6. Human-operated turning*

In order to show that the robotic fish can turn around by repeatedly swinging and bending the caudal fin, we operated the robot manually. The human-operation has been conducted using the controller box with joysticks.[21] Through the swing of the joystick, the initial phase of the voltage applied to the stator can be shifted from $-1800^{o}$ to $+1800^{o}$. Figure 14 illustrates the trajectories of left and right turning, where a target marker attached to the dorsal fin has been used for tracking. It is demonstrated that the robotic fish is capable of implementing highly smooth turning through manual operation.

## 5. Conclusions and Future Research

We have fabricated a series of robotic fish using electrostatic film motors. In the present paper, some of the disadvantages of previous robotic fish have been described, and solutions to these problems have been proposed. In the redesigned robotic fish, polyurethane rubber was used as the waterproofing material to prevent silicon oil from being absorbed. The present robotic fish was redesigned six months ago, its waterproof coating has not yet started to decay. An elaborate linear guide mechanism was adopted in order to avoid the pitch angular deflection between the stator and slider films. In addition, we not only designed an improved prototype of our robotic fish, but also experimentally evaluated the relationship between its locomotion and motor control parameters. In our previous studies, we focused simply on verifying the feasibility of the application of a novel electrostatic film motor to a light and flexible power distribution system (e.g., robotic fish) and did not implement more sophisticated detection. However, it is essential to investigate dynamics for improving maneuverability and achieving fish-like performance. Therefore, we clarified the relationship between the control parameters of the motor and locomotion properties through experiments in the present paper. Even though there is one active caudal fin in the robotic fish, it is capable of tuning cruising speed, emerging, submerging, and sharp turning by appropriately adjusting the amplitude of frequency sweeping, sweeping cycle period, and initial phase. These results facilitate the establishment concerning the fundamental control principles of the robotic fish locomotion.

The present paper has experimentally evaluated the proposed open-loop swimming control method. Further details about the propulsion hydrodynamic forces on the swinging caudal fin should be studied by varying the fin morphological parameters and fin motion kinematics in the future research. Even so, a number of formulas about the prototype design and motion optimization have been developed, which will provide a reference for future research. In addition, energy efficiency is of crucial importance for robot design, because it is an essential machine evaluation index. Thus, a significant energetic improvement should also be conducted in our ongoing work. As described in our previous study,[21] the operation signal for the electrostatics film motor is powered by power amplifiers and then boosted to high voltage by transformers. On the other hand, the unique electrostatic film motor can be considered to be a capacity load. Therefore, we can use the resonance between the inductance of the secondary circuit of the transformers and the capacitance of the motor so as to reduce the reactive current in the power supply circuit. Next, the optimum driving frequency causing the resonance should be examined from the viewpoint of energy efficiency. Furthermore, future research will investigate a bio-inspired control strategy (e.g., neural feedback).

## Appendix A: Analysis About Cruising speed

A simple analysis is used to estimate the relation between the cruising speed and the motion of the electrostatic film motors. As shown in Fig. 15, the following hypotheses are adopted to derive the analysis: (1) the elaborate power transmission system (see Fig. 5(b)) is considered to be a simple mechanism where two plastic films of the caudal fin are flat without deformation and they can pivot, respectively, on the corners of sponges at the ends of the two slider films; (2) the cruising speed is in proportion to the swing range of the caudal fin;

https://doi.org/10.1017/S0263574709005694 Published online by Cambridge University Press

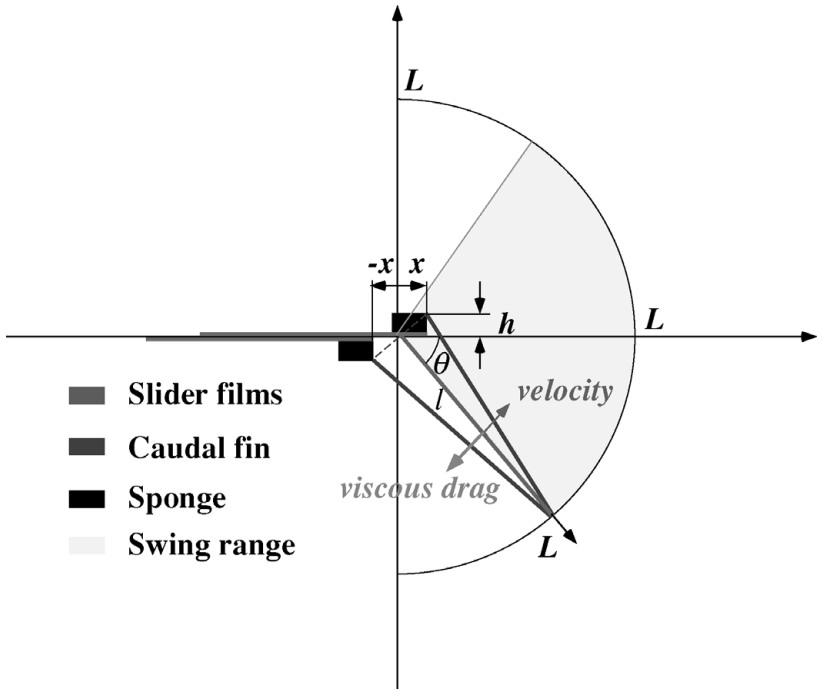


Fig. 15 Schematic of theoretical analysis.

(3) the swing range of the caudal fin is a sector with a radius $L$; and (4) the swing angle $\theta$ is tiny.

By inspection, the swing angle of the caudal fin is

$$\tan\theta = \frac{x}{h}. \tag{A.1}$$

Due to the hypothesis (4), the swing angle can be expressed as

$$\theta = \frac{x}{h}, \tag{A.2}$$

$$\mathrm{d}\theta = \frac{\mathrm{d}x}{h}, \tag{A.3}$$

where $h$ denotes the thickness of the sponge and $x$ indicates the moving distance of the slider films. Based on the frequency modulation of the voltage formulated in Eq. (3), we calculated the moving speed of the slider film

$$\begin{aligned}\frac{\mathrm{d}x}{\mathrm{d}t} &= 4p_{\mathrm{st}}(f_{\mathrm{st}} - f_{\mathrm{sl}}) \\ &= 4p_{\mathrm{st}}A\sin\left(\frac{2\pi}{T_{\mathrm{sw}}}t\right).\end{aligned} \tag{A.4}$$

The Eq. (A.3) and Eq. (A.4) lead to the swing angular velocity,

$$\mathrm{d}\theta = \frac{4p_{\mathrm{st}}A}{h}\sin\left(\frac{2\pi}{T_{\mathrm{sw}}}t\right)\mathrm{d}t. \tag{A.5}$$

Thus, the swing range of the caudal fin is given as

$$S = \frac{1}{T_{\mathrm{sw}}}\int \pi L^2\frac{|\mathrm{d}\theta|}{2\pi}. \tag{A.6}$$

Substituting Eq. (A.5) into Eq. (A.6), we obtain

$$\begin{aligned}S &= \frac{1}{T_{\mathrm{sw}}}\int_0^{T_{\mathrm{sw}}} \pi L^2\cdot\frac{1}{2\pi}\cdot\frac{4p_{\mathrm{st}}A}{h}\left|\sin\left(\frac{2\pi}{T_{\mathrm{sw}}}t\right)\right|\mathrm{d}t \\ &= \frac{2L^2p_{st}A}{T_{\mathrm{sw}}h}\int_0^{T_{\mathrm{sw}}}\left|\sin\left(\frac{2\pi}{T_{\mathrm{sw}}}t\right)\right|\mathrm{d}t \\ &= \frac{8L^2p_{\mathrm{st}}A}{T_{\mathrm{sw}}h}\int_0^{\frac{T_{\mathrm{sw}}}{4}}\sin\left(\frac{2\pi}{T_{\mathrm{sw}}}t\right)\mathrm{d}t \\ &= \frac{8L^2p_{\mathrm{st}}A}{T_{\mathrm{sw}}h}\cdot\frac{T_{\mathrm{sw}}}{2\pi}\left[-\cos\left(\frac{2\pi}{T_{\mathrm{sw}}}t\right)\right]_0^{\frac{T_{\mathrm{sw}}}{4}} \\ &= \frac{4L^2p_{\mathrm{st}}}{\pi h}\cdot A.\end{aligned} \tag{A.7}$$

Because of the hypothesis (2), Eq. (A.7) shows that the cruising speed of the robotic fish is in proportion to the amplitude of frequency sweeping of the driving voltage. Namely, the cruising speed is increased as the swing speed and swing period of the caudal fin increases.

## Appendix B: Analysis About Thrust Force of Motors

Referring to Fig. 15, we must simply consider the caudal fin to be a flat plate (i.e., the gray line in the caudal fin). We introduce the damping coefficient as c. Then, the damping coefficient at the minute section $dl$ is c$dl$. Thus, we obtain the viscous drag and swing velocity at the minute section $dl$ as

$$F_{\mathrm{vd}} = (\mathrm{c}dl)\cdot l\cdot\frac{\mathrm{d}\theta}{\mathrm{d}t},$$

https://doi.org/10.1017/S0263574709005694 Published online by Cambridge University Press

$$v_{\mathrm{sw}} = l\frac{\mathrm{d}\theta}{\mathrm{d}t}. \tag{B.1}$$

At the length $L$ of the caudal fin, we simply calculate the workload of the caudal fin as follows,

$$\begin{aligned} P_{fin} &= \int_0^L F_{vd} \cdot v_{\mathrm{sw}} \\ &= \int_0^L \mathrm{c}dl \cdot l \cdot \frac{\mathrm{d}\theta}{\mathrm{d}t} \cdot \left(l\frac{\mathrm{d}\theta}{\mathrm{d}t}\right) = \int_0^L \mathrm{c}l^2 \left(\frac{\mathrm{d}\theta}{\mathrm{d}t}\right)^2 \mathrm{d}l \\ &= \left[\frac{1}{3}\mathrm{c}l^3 \left(\frac{\mathrm{d}\theta}{\mathrm{d}t}\right)^2\right]_0^L = \frac{1}{3}\mathrm{c}L^3 \left(\frac{\mathrm{d}\theta}{\mathrm{d}t}\right)^3 \\ &= \frac{1}{3}\mathrm{c}\frac{L^3}{h^2}\left(\frac{\mathrm{d}x}{\mathrm{d}t}\right)^2, \end{aligned} \tag{B.2}$$

where Eq. (A.3) is applied to this calculation. On the other hand, the thrust force of each slider is set as $f_1$ and $f_2$, respectively. The power of the electrostatic film motor can be calculated as

$$P_{\mathrm{motor}} = (f_1 + f_2)\frac{\mathrm{d}x}{\mathrm{d}t}. \tag{B.3}$$

If the power of the motor is sufficient to the workload of the caudal fin (i.e., $P_{\mathrm{fin}} = P_{\mathrm{motor}}$), the desired thrust force of the slider $f_d = (f_1 = f_2)$ should satisfy the following relation,

$$2f_d = f_1 + f_2 = \frac{1}{3} \cdot \mathrm{c} \cdot \frac{L^3}{h^2}\left(\frac{\mathrm{d}x}{\mathrm{d}t}\right). \tag{B.4}$$

Hence,

$$f_d = \frac{\mathrm{c}L^3}{6h^2}\left(\frac{\mathrm{d}x}{\mathrm{d}t}\right). \tag{B.5}$$

As expressed in Eq. (B.5), the desired thrust force of the slider is in inverse proportion to the square of the sponge thickness $h$. In fact, it was observed in our experiment that swing motion of the caudal fin became easier as we thickened the sponge connecting the films of the slider and the caudal fin.

## Appendix C: List of Notation

| | |
|---|---|
| $A$ | amplitude of frequency sweeping |
| $L$ | radius of swing range of the caudal fin |
| $P_{\mathrm{motor}}$ | power of the electrostatic film motor |
| c | damping coefficient |
| $f_{\mathrm{d}}$ | desired thrust force of the motor |
| $f_{\mathrm{st}}$ | frequency of voltage on the stator |
| $l$ | length along with the caudal fin |
| $p_{\mathrm{st}}$ | electrode pitch of the stator |
| $v_{1\sim6}$ | voltages applied to $1 \sim 6$ electrodes |
| $v_{\mathrm{st}}$ | voltage amplitude on the stator |
| $x$ | moving distance of the slider film |
| $\phi$ | phase shift of voltage |
| $F_{\mathrm{vd}}$ | viscous drag at the minute section $dl$ |
| $P_{\mathrm{fin}}$ | workload of the caudal fin |
| $T_{\mathrm{sw}}$ | frequency sweeping cycle period |
| $f_{1\sim2}$ | thrust force of the slider $1 \sim 2$ |
| $f_{\mathrm{sl}}$ | frequency of voltage on the slider |
| $h$ | thickness of the sponge |
| $p_{\mathrm{sl}}$ | electrode pitch of the slider |
| $u$ | slider running speed |
| $v_{\mathrm{sl}}$ | voltage amplitude on the slider |
| $v_{\mathrm{sw}}$ | swing velocity at the minute section $dl$ |
| $\theta$ | swing angle of the caudal fin |
| $\phi_{\mathrm{ref}}$ | target value of the phase shift |

## Acknowledgements

The present study was supported by the Creation and Support Program for Start-ups from the University of the Japan Science and Technology Agency and by a Grant-in-Aid for Scientific Research on Priority Areas, #16078203, from MEXT of Japan. Zu Guang Zhang's work was supported by the Aid-Fund for Encouraging Research at Tokyo University of Science.

## References

1. C. M. Breder, "The locomotion of fishes," *Zoologica* **4**, 159–256 (1926).
2. J. E. Colgate and K. M. Lynch, "Mechanics and control of swimming: A review," *IEEE J. Oceanic Eng.* **29**(3), 660–673 (2004).
3. M. Sfakiotakis, D. M. Lane and J. B. C. Davies, "Review of fish swimming modes for aquatic locomotion," *IEEE J. Oceanic Eng.* **24**, 237–252 (1999).
4. M. S. Triantafyllou and G. S. Triantafyllou, "An efficient swimming vehicle," *Sci. Am.* **272**, 40–46 (1995).
5. I. Yamamoto and Y. Terada, "Robotic Fish and its Technology," *Proceedings of SICE Annual Conference*, Fukui, Japan (2003) pp. 342–345.
6. K. Hirata, "Development of Experimental Fish Robot," *Proceedings of IEEE International Symposium on Marine Engineering*, Tokyo, Japan (2000) pp. 711–714.
7. J. D. Liu and H. S. Hu, "Mimicry of Sharp Turning Behaviours in a Robotic Fish," *Proceedings of IEEE International Conference on Robotics and Automation*, Barcelona, Spain (2005) pp. 3329–3334.
8. J. D. Liu, I. Dukes and H. S. Hu, "Novel Mechatronics Design for a Robotic Fish," *Proceedings of IEEE/RSJ International Conference on Intelligent Robots and Systems,* Edmonton, Canada (2005) pp. 2077–2082.
9. D. Lachat, A. Crespi and A. J. Ijspeert, "Boxybot: A Swimming and Crawling Fish Robot Controlled by a Central Pattern Generator," *Proceedings of IEEE/RAS-EMBS International Conference on Biomedical Robotics and Biomechatronics*, Pisa, Italy (2006).
10. P. Kodati, J. Hinkle and X. Deng, "Micro Autonomous Robotic Ostraciiform (marco): Design and Fabrication," *Proceedings of IEEE International Conference on Robotics and Automation,* Rome, Italy (2007) pp. 960–965.
11. D. S. Barrett, M. S. Triantafyllou, D. K. P. Yue, M. A. Grosenbaugh and M. J. Wolfgang, "Drag reduction in fish-like locomotion," *J. Fluid Mech.* **392**, 183–212 (1999).
12. S. Guo, T. Fukuda and K. Asaka, "A new type of fish-like underwater microrobot," *IEEE/ASME Trans. Mechatronics* **8**, 136–141 (2003).

https://doi.org/10.1017/S0263574709005694 Published online by Cambridge University Press

13. N. Shinjo and G. W. Swain, "The use of shape memory alloy for the design of oscillatory propulsion system," *IEEE J. Oceanic Eng.* **29**, 750–755 (2004).
14. M. G. Borgen, G. N. Washington and G. L. Kinzel, "Design and evolution of a piezoelectrically actuated miniature swimming vehicle," *IEEE/ASME Trans. Mechatronics* **8**, 66–74 (2003).
15. J. Naciri, A. Srinivasan, W. Sandberg, R. Ramamurti and B. Ratna, "Nematic Liquid Crystal Elastomers as Artificial Muscles," *Proceedings of International Symposium on Unmanned Untethered Submersible Technology,* Durham, USA (2003) pp. 295–299.
16. J. Paquette and K. J. Kim, "Ionomeric electro-active polymer artificial muscle for naval applications," *IEEE J. Oceanic Eng.* **29**, 729–737 (2004).
17. T. Niino, A. Yamamoto and T. Higuchi, "Operation of a dual excitation multiphase electrostatic drive by amplitude-modulated ac voltage," *Electr. Eng. Japan* **131**(4), 78–84 (2000).
18. A. Yamamoto, T. Niino and T. Higuchi, "Modeling and identification of an electrostatic motor," *Precis. Eng.* **30**, 104–113 (2006).
19. N. Yamashita, Z. G. Zhang, A. Yamamoto, M. Gondo and T. Higuchi, "Voltage-induction type electrostatic film motor driven by two- to four-phase ac voltage and electrostatic induction," *Sensors Actuators: A* **140**(2), 239–250 (2007).
20. Z. G. Zhang, N. Yamashita, M. Gondo, A. Yamamoto and T. Higuchi, "Electrostatically actuated robotic fish: Design and control for high-mobility open-loop swimming," *IEEE Trans. Robot.* **24**(1), 118–129 (2008).
21. Z. G. Zhang, N. Yamashita, A. Yamamoto and T. Higuchi, "Development of a robotic fish using electrostatic film motors: The seidengyo II robot," *Adv. Robot.* **21**(15), 1787–1803 (2007).
22. M. H. Dickinson, C. T. Farley, R. J. Full, M. A. R. Koehl, R. Kram and S. Lehman, "How animals move: An integrative view," *Science* **288**, 100–106 (2000).

https://doi.org/10.1017/S0263574709005694 Published online by Cambridge University Press